Extraction of Intrinsic Parameters of Lead–Acid Batteries Using Energy Recycling Technique

Chun-Sing Cheng, *Student Member, IEEE*, Ricky Wing-Hong Lau, *Senior Member, IEEE*, Nand Kishor Rathi, and Henry Shu-Hung Chung, *Fellow, IEEE*

***Abstract*—This paper presents the use of an energy recycling technique to extract the intrinsic parameters of lead–acid batteries. The charging and discharging currents of the battery under test are programmed by controlling a bidirectional dc–dc converter to profile the power flow between the battery and a supercapacitor. The sampled battery voltage and current information over the charging and discharging periods are used to estimate the parameters of a high-order electrical battery model with a modified particle swarm optimization algorithm and compare with the battery voltage and current predicted with the extracted parameters. With the energy recycling mechanism, the proposed parameter extraction process is environment friendly and has low power dissipation, thus increasing the power handling density and allowing long testing duration. A prototype that can extract the intrinsic parameters of eight different types of 12 V, 130 A lead–acid batteries has been built. Its performance has been evaluated with different charging and discharging profiles. The estimated parameters are favorably verified with the theoretical predictions, results obtained by the extended Kalman filter method, and results obtained on a calibrated commercial battery testing system. Results reveal that testing batteries with both charging and discharging processes gives a more accurate prediction of battery performance.**

***Index Terms*—Batteries, battery parameters, computational intelligence, energy storage, machine intelligence, optimization, particle swarm optimization (PSO).**

NOMENCLATURE

v_b	Battery voltage.
i_b	Battery current.
C_o	Supercapacitor in the bidirectional dc–dc converter.
R_c	Equivalent series resistance of C_o.
L	Inductor in the converter.
R_L	DC resistance of L.

Manuscript received January 26, 2018; revised June 3, 2018; accepted August 8, 2018. Date of publication August 14, 2018; date of current version March 29, 2019. This work was supported in part by a grant from the City University of Hong Kong, through Project #7004841, and in part by Premier Technologies Limited. This paper was presented in part at the IEEE Energy Conversion Congress and Exposition, Milwaukee, WI, USA, Sep. 18–22, 2016. Recommended for publication by Associate Editor B. Semail. *(Corresponding author: Henry Shu-Hung Chung.)*

C.-S. Cheng, R. W.-H. Lau, and H. S.-H. Chung are with the Centre for Smart Energy Conversion and Utilization Research, City University of Hong Kong, Hong Kong (e-mail:

determining SOC. However, the entire process is time-intensive, and causes energy wastage and impact on the battery's life cycle. To shorten the testing period, the open-circuit voltage (OCV) method estimates the SOC with the measured OCV and OCV-SOC curve [28]. However, the battery needs to be disconnected from the load to conduct lengthy relaxation.

As discussed in [29], battery impedance gives an effective measure of SOH. Several methods, based on measuring dc resistance or ac impedance, have been proposed. In measuring the dc resistance, the battery is subject to current pulses. The dc resistance is estimated by studying the momentarily change of the terminal voltage [5]. The SOH is evaluated by using the variation of the measured dc resistance with respect to its nominal value [6], [30]. The ac impedance of the battery is typically used to characterize battery dynamics, electrochemical reaction, and material properties. The test is conducted by charging or discharging the battery with a small-signal perturbation of adjustable excitation frequency. The ac impedance is estimated by using the battery voltage and current at the frequency of interest. Among various techniques, EIS has been widely adopted. However, it is time consuming and requires using sophisticated equipment. It is thus suitable for offline measurement.

Several time-efficient online measurement methods, such as injection of single ac sinusoidal wave [8], background noise [9], or white noise [10] into in the excitation signals, are suggested. The magnitude and phase angle of the impedance are estimated by the sampled battery voltage and current information. Those methods require conducting multiple high-precision measurements, as the signals are small and time-varying. Thus, many sum-of-sines signal with single period methods, including compensated synchronous detection (CSD) [17], [18], harmonic CSD [19], [20], and optimized broadband impedance spectroscopy [21], have been proposed to obtain battery conditions rapidly and overcome noise ratio issue. The signals comprise a few frequencies within the range of interest. They are of the same excitation amplitude. However, the frequencies have to be selected carefully, such as octave bands, to avoid possible crosstalk.

Hybrid pulse power characterization can measure the power capability of the battery under test. It is conducted by applying high charging and discharging current pulses for a period of time, such as 18 s in emulating battery operations on electric vehicles in [27]. The abilities of accepting charges and delivering currents are identified. However, the dynamical characteristics of the battery cannot be fully extracted in the entire process.

Many estimation methods, such as genetic algorithms (GAs) [33], extended Kalman filter (EKF) [34]–[36], and particle swarm optimization (PSO) [37], have been proposed to evaluate battery parameters. Among them, GA is the most accurate method, but its implementation is complex and requires considerable computational resources. EKF has been widely adopted in dealing with estimation problems, due to its fast convergence speed and simple implementation. However, its performance will degrade if the model, level of noise, and initial guess are uncertain [34], [38]. Many enhanced approaches have been proposed to increase the robustness of EKF [33]–[36], [38]. PSO, which is inspired by swarm's behavior, is simple in operation and is applicable for tackling many optimization problems. However, it would sometimes be trapped into local optima [37].

To conclude, the above methods have tradeoff among speed, accuracy, and implementation complexity. Their main challenges are listed as follows.

1) It is necessary to handle the energy discharged from the battery under test to the dummy load throughout the test.
2) The testing duration has to make compromise with the power dissipation and thermal management. The testing results may not be able to observe the effects of the intrinsic parameters of long time constants.
3) Either charging or discharging characteristic, but not both, is taken in the test.
4) No large-signal characteristics are considered. As discussed in [39]–[41], large-signal information is crucial, because some intrinsic parameters of the battery vary with different discharging rates and operating points.
5) The estimation accuracy would be affected by initial guess [33], [34].
6) The estimated parameters would sometimes be trapped into local optima [37].

To deal with the above challenges, an energy and computational efficient intrinsic parameter estimation technique is presented. By controlling the power flow between the battery under test and a supercapacitor through a bidirectional dc–dc converter, the battery current profile and operating mode are controlled. The method is ideally nondissipative and allows testing large-signal battery behaviors over a long period of time. As the measurable electrical quantities include battery voltage and current only, a modified PSO (m-PSO) [36]–[38], which is a computational intelligence technique for dealing with black-box problems, is used to estimate the parameters of a second-order electrical model for characterizing battery performance and condition. This approach gives a good balance between accuracy and computational speed, suitable for life expectancy estimation.

A prototype for extracting the intrinsic parameters of eight different types of 12 V, 130 A lead–acid batteries has been built. Its performance has been evaluated with different charging and discharging patterns. The estimated parameters are compared with the theoretical predictions and the results obtained by a calibrated commercial battery testing system. The performance of the proposed m-PSO method will be compared with that of the EKF method [34], [36], [42].

II. System Architecture

Fig. 1 shows the system architecture. A bidirectional dc–dc converter is connected between the battery under test and the supercapacitor C_o. The battery is modeled by a state-of-charge (SOC)-dependent capacitor $C(\mathrm{SOC})$ for characterizing the nonlinear relationship between the electromotive force and SOC, a series resistor R_0 for modeling instantaneous voltage drop upon a sudden load change, and two *RC* networks for characterizing steady-state and transient behaviors [37].

The bidirectional dc–dc converter is formed by two semiconductor switches, MOS1 and MOS2, and an inductor L. When

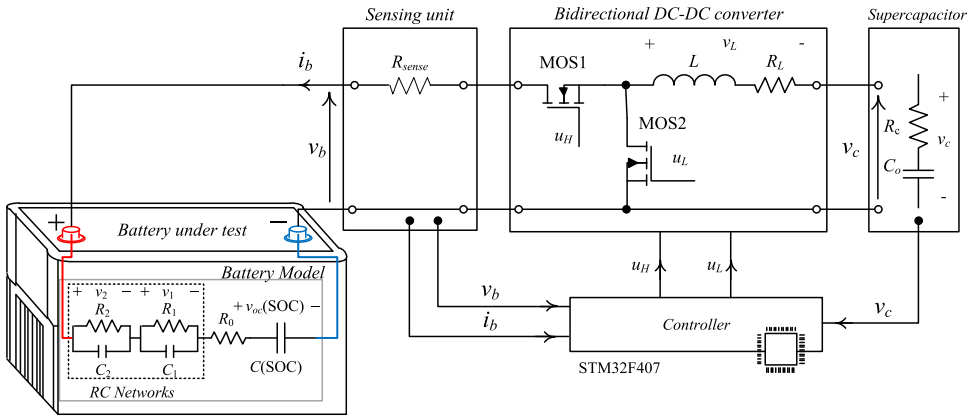

Fig. 1. System architecture.

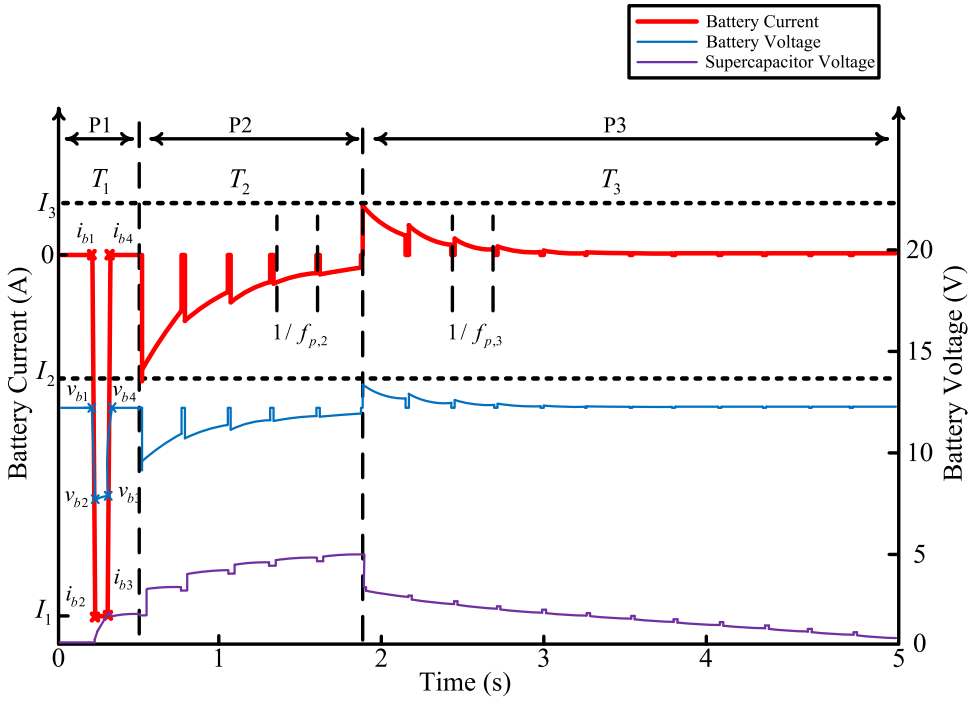

Fig. 2. Testing profiles with charging and discharging processes.

the battery discharging behavior is studied, the converter is operated as a buck converter and is programmed to transfer energy from the battery to C_o. Conversely, when the battery charging behavior is studied, the converter is operated as a boost converter and is programmed to transfer energy from C_o to the battery. The entire charging and discharging profiles are controlled by a microcontroller unit.

Fig. 2 shows the waveforms of the battery voltage, v_b, battery current, i_b, and voltage across C_o, v_c, under a sequence of programmed charging and discharging profiles. The battery is first tested with a high discharging current—profile P1. The duration of this process is T_1 and the discharging current is designed to be larger than I_1. This stage is used to test the power delivery capability of the battery and provide the m-PSO algorithm with the information about the searching boundaries for R_0. The battery voltage and current before and after this process, including v_{b1}, v_{b2}, v_{b3}, v_{b4}, i_{b1}, i_{b2}, i_{b3}, and i_{b4}, as shown in Fig. 2, are sampled. v_c will increase in this stage.

After conducting P1, the battery will then be tested with the second profile P2, which is also a discharging process. The duration of this process is T_2. The initial discharging current is I_2. A high-frequency current perturbation is injected. The perturbation frequency is $f_{p,2}$. The function of this stage is to extract the parameters of the *RC* networks under the discharging process. v_b and i_b are sampled at the sampling frequency of f_s throughout this process. v_c will continue to increase.

After conducting P2, the battery will be tested with the third profile P3, which is a charging process. The duration of this process is T_3. The initial discharging current is I_3. Again, a high-frequency current perturbation is injected. The perturbation

frequency is $f_{p,3}$. The function of this stage is to extract the parameters of the *RC* networks under the charging process. v_b and i_b are also sampled at the sampling frequency of f_s throughout this process. v_c will start discharging.

Profiles P2 and P3 are conducted repeatedly for N times. The duration of the whole testing process is T.

The bidirectional dc–dc converter is operated differently in generating the three profiles. In conducting P1, MOS1 is fully turned ON, while MOS2 is fully turned OFF. The battery is connected to C_o directly. As $v_b > v_c$, a high discharging current for testing the delivery capability of the battery will appear. Since the duration of this testing profile is short, as compared to the time constant of the *RC* networks, the battery current can be expressed as follows:

$$i_b(t) \approx \frac{V_{OC}}{2L(\sqrt{\alpha^2-\omega^2})}\left(e^{t(-\alpha+\sqrt{\alpha^2-\omega^2})}+e^{t(-\alpha-\sqrt{\alpha^2-\omega^2})}\right) \tag{1}$$

where $\alpha = (R_{\text{sense}} + R_{\text{on}} + R_L + R_c)/2L$ and $\omega^2 = \frac{1}{LC_o}$.

There is a voltage drop in conducting this profile. v_b is changed from v_{b1} to v_{b2} and i_b is changed from i_{b1} to i_{b2}. The value of R_0 can be approximated by

$$R_0 \approx \frac{v_{b2}-v_{b1}}{i_{b2}-i_{b1}}. \tag{2}$$

Thus, the magnitude of the voltage drop can give the order of R_0, thus, indicating how well the battery can deliver a high current in a short period of time.

In conducting P2, the converter is operated as a synchronous buck converter in continuous conduction mode (CCM) with the battery as the source and C_o as the load. The battery current is programmed to ensure that C_o will not be overcharged. The duration of this profile is sufficiently longer than the shortest time constant of the two *RC* networks.

In conducting P3, the converter is operated as a synchronous boost converter in CCM with C_o as the source and the battery as the load. The battery current is programmed to ensure that C_o will be fully discharged before the end of this profile. The duration of this profile is sufficiently longer than the shortest time constant of the two *RC* networks.

Thus, profiles P2 and P3 are combined to form an energy recycling process to test battery behaviors. In addition, they will be repeated for a duration longer than the longest time constant of the two *RC* networks.

III. Simplified Design Procedure

The bidirectional dc–dc converter comprises three main power components, including the switching devices, MOS1 and MOS2, supercapacitor C_o, and inductor L. They are designed by considering the minimum battery voltage $v_{b,\min}$, maximum battery voltage $v_{b,\max}$, maximum battery current $i_{b,\max}$, and maximum supercapacitor voltage $v_{c,\max}$.

Step 1: Design the value for C_o

Assume that all energy from the battery is transferred to C_o in conducting P1. Thus, by applying the conservation of energy

$$C_o \geq \frac{2\, v_{b,\max}\, i_{b,\max}\, T_1}{{v_{c,\max}}^2}. \tag{3}$$

Step 2: Design the value for L

Assume that the ON-state resistances of MOS1, MOS2, and R_L are neglected. Consider that the inductor current ripple is 20% of the maximum output current and the converter is in CCM in generating the P2 [43]. Thus

$$L \geq \frac{v_{c,\max}(1-\frac{v_{c,\max}}{v_{b,\max}})}{0.2 f_{\text{sw}}\frac{v_{b,\max}-v_{c,\max}}{R_c}}. \tag{4}$$

Step 3: Design the maximum allowable ON-state resistance for MOS1 and MOS2

The value of R_{on} has to be limited to a value that can generate the necessary high current pulse in conducting P1. As the duration of the P1 is short, the variation of the battery current is neglected. Based on (1)

$$R_{\text{on}} < \sqrt{\frac{{v_{b,\min}}^2}{{i_{b,\min}}^2}+\frac{4L}{C}} - R_c - R_L - R_{\text{sense}}. \tag{5}$$

Equation (5) gives the maximum value of the ON-state resistance for MOS1 and MOS2.

IV. m-PSO Algorithm for Parameter Extraction

PSO, which is inspired by swarm's behavior [35], consists of a population of particles. Each particle comprises a set of parameters as depicted in (6) below. Particles will move around the search space through some operators and search for the global best solution. Each particle will change its velocity toward the best solution associated with other particles. The proposed m-PSO method is based on PSO with random perturbation particles and searching boundary definition of battery characteristics for higher global solution search ability and faster convergence speed. Traditionally, the best particle does not have any reference to adjust its trajectory. It may cause the swarm trapping into local optima. In the m-PSO, the random perturbation particle improves the best particle by providing an extra solution at each time step. The new solutions help the swarm jump out of the local optima and accelerate the search. The range of search boundary for R_0 is reduced by referencing (2). The convergence time and the required data size in the parameter estimation are reduced.

The proposed mechanism of determining the battery parameters is shown in Fig. 3(a). It consists of two main functional blocks including the battery voltage estimator (BVE) and m-PSO engine. The two blocks are linked by a set of parameters P

$$P = \{\text{SOC}(0), R_0, R_1, R_2, \tau_1, \tau_2, v_1(0), v_2(0)\}. \tag{6}$$

The BVE is used to calculate the time series of v_b with the sampled time series of the actual battery current and the parameters provided by the m-PSO engine. The function of the m-PSO engine is used to estimate the parameters by minimizing the errors between the time series of the actual and calculated battery voltage. Such error can be considered as a measure of fitness in the estimation. The open-circuit voltage of the battery, $v_{\text{OC}}(\text{SOC})$, for the BVE is obtained from the v_{OC}-SOC characteristics, which are obtained experimentally by discharging the

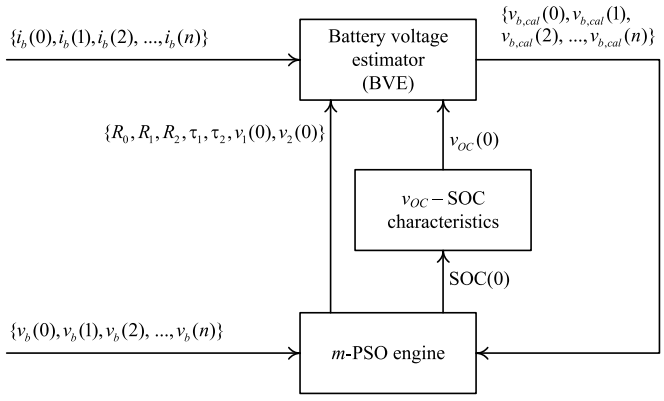

(a)

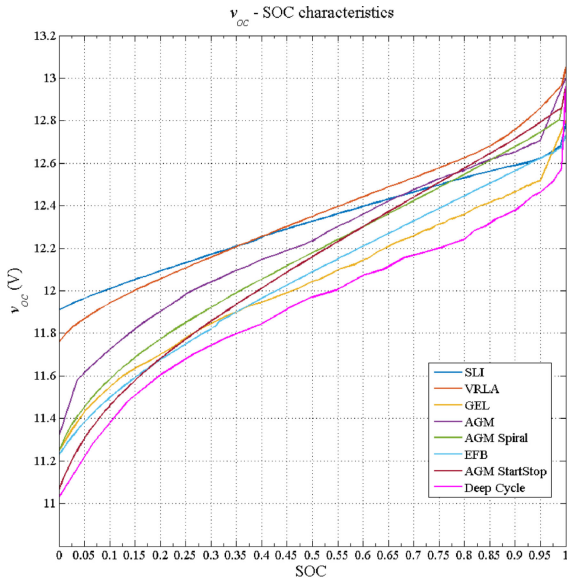

(b)

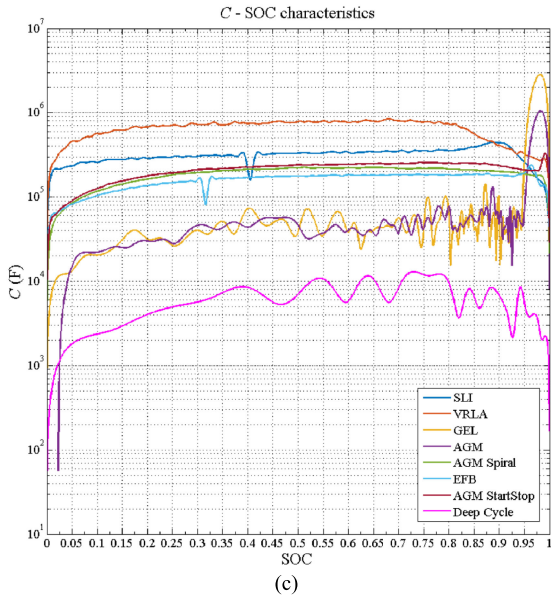

(c)

Fig. 3. Mechanism for determining battery parameters. (a) Mechanism. (b) Typical $v_{\rm oc}$ – SOC characteristics. (c) C – SOC characteristics.

battery from float voltage to cutoff voltage at constant current, where the float voltage is the voltage that is required to maintain a battery full charged such as 13.5 V for valve-regulated lead–acid (VRLA) batteries and the cutoff voltage is the voltage that a battery is considered fully discharged and should not discharge any longer, for example, 10.5 V for starting-lighting-ignition (SLI) batteries. First, the battery is charged to float voltage at a constant current (C/10) and held at the float voltage until the current has dropped below C/60. After resting for 2 h, the battery is then discharged at the rate of C/10. The discharging process is interrupted in every 300 s and the open-circuit voltage of the battery is measured after resting for 600 s [3]. After the measurement, the discharging process is continued and the process is repeated until the battery voltage has reached the cutoff voltage.

The characteristics of eight typical lead–acid batteries are shown in Fig. 3(b). They are SLI, VRLA, gelified electrolyte (GEL), absorbent glass mat (AGM), absorbent glass mat with spiral structure (AGM Spiral), enhanced flooded battery (EFB), absorbent glass mat with start–stop functionality (AGM Start-Stop) and deep cycle battery. The operations of the BVE and m-PSO are given below.

A. Battery Voltage Estimator (BVE)

SOC is defined as the ratio between the charges Q stored in the battery and the fully-charged capacity Q_o. An SOC-dependent capacitor $C(\mathrm{SOC})$ is defined as follows [37]:

$$C(\mathrm{SOC}) = \frac{d\,Q(\mathrm{SOC})}{d\,v_{\rm oc}(\mathrm{SOC})} = Q_o\,\frac{d\,\mathrm{SOC}}{d\,v_{\rm oc}(\mathrm{SOC})}. \tag{7}$$

Thus, the value of C at different SOC is obtained by determining the slope of the $v_{\rm oc}$-SOC curve in Fig. 3(b) together with the value of Q_o. Fig. 3(c) shows the value of C against SOC.

Based on Kirchhoff's voltage law, the voltages on the two *RC* networks are as follows:

$$v_1(t) = \frac{1}{C_1}\int_0^t \left[i_b(\theta) - \frac{v_1(\theta)}{R_1}\right] d\theta + v_1(0) \tag{8}$$

and

$$v_2(t) = \frac{1}{C_2}\int_0^t \left[i_b(\theta) - \frac{v_2(\theta)}{R_2}\right] d\theta + v_2(0) \tag{9}$$

where $v_1(t)$ and $v_2(t)$ are the voltages across C_1 and C_2, respectively.

The terminal voltage of the battery v_b can be expressed as follows:

$$v_b(t) = v_{\rm oc}[\mathrm{SOC}(t)] + i_b(t)\,R_0 + v_1(t) + v_2(t) \tag{10}$$

where $v_{\rm oc}[\mathrm{SOC}(t)] = \int_0^t \frac{i_b(\theta)}{C[\mathrm{SOC}(\theta)]}d\theta + v_{\rm oc}[\mathrm{SOC}(0)]$ and $\mathrm{SOC}(\theta)$ is the SOC at time θ.

Hence, the BVE estimates the time series of the battery voltage with (8)–(10) with the parameters estimated by m-PSO and the $v_{\rm oc}$-SOC characteristics.

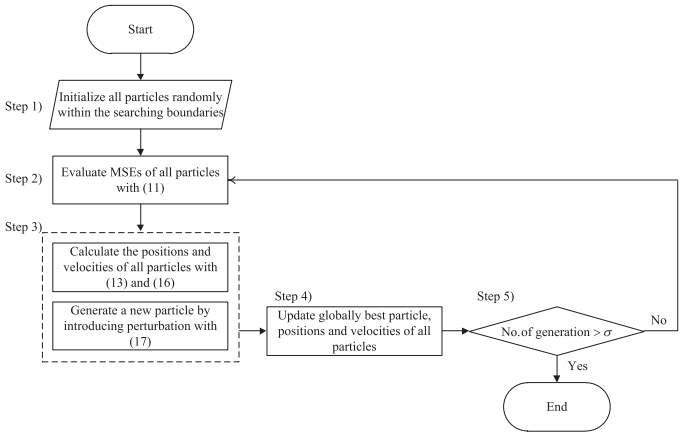

Fig. 4. Flowchart of the m-PSO algorithm.

B. m-PSO Engine

The m-PSO engine is used to determine the values of the parameters defined in P [i.e., (6)] for minimizing the mean square error (MSE) between the actual battery voltage $v_b(t)$ and the calculated battery voltage $v_{b,\mathrm{cal}}(t)$ over T. The objective function and the procedure of the m-PSO are described as follows.

1) Objective Function: The MSE for a given set of parameter P is defined by averaging the sum of the square of the errors between the actual $v_b(t)$ and $v_{b,\mathrm{cal}}(t)$ over the testing period T. That is

$$\mathrm{MSE}(P) = \frac{1}{T}\int_0^T \left(v_b(t) - v_{b,\mathrm{cal}}[t, P, i_b(t)]\right)^2 \mathrm{d}t. \tag{11}$$

The best set of parameters, P_0, in (6), gives the minimum MSE(P)

$$P_0 = \underset{P}{\arg\min}\ \mathrm{MSE}(P). \tag{12}$$

2) m-PSO Algorithm: Fig. 4 shows the flowchart of the algorithm. n is the population size, that is, the number of candidates (possible solutions) for P. σ is the total number of generations (optimization cycles) in the optimization process. Each candidate is a particle, which holds its position (set of parameters) P_i and velocity v_i. To reduce the convergence time and the required data size in the parameter estimation, the internal resistance R_0 is approximated by (2) for defining the search boundary. According to the cell capacity study in [30], the upper and lower boundaries of R_0 are set as 150% and 50% of the estimated value, respectively.

In each generation, the parameters in each particle is updated or generated by considering its velocity, which is calculated by considering several factors, including its velocity in the last generation, its position from the globally best particle (solution set) so far, and its position from its best particle in the last generation. Mathematically, the velocity v_i in the gth optimization generation, $v_i^{(g)}$, is defined as follows:

$$\begin{aligned} {v_i}^{(g)} = {}& w^{(g-1)}\ {v_i}^{(g-1)} + 2\ {r_{1,i}}^{(g-1)}\ [P_G - P_i^{(g-1)}] \\ & + 2\ {r_{2,i}}^{(g-1)}\ [{P_{H,i}}^{(g-1)} - P_i^{(g-1)}] \end{aligned} \tag{13}$$

where ${v_i}^{(g-1)}$ is the velocity of the ith particle in the $(g-1)$th generation, P_G is the globally best particle in the search so far, $P_i^{(g-1)}$ holds the position of the ith particle in the $(g-1)$th generation, ${P_{H,i}}^{(g-1)}$ holds the best position found by the ith particle in the $(g-1)$th generation, $w^{(g-1)} \in (0,1)$ is the learning factor and $r_{1,i}^{(g-1)}$ and $r_{2,i}^{(g-1)}$, initialized randomly, are weighting factors evenly distributed between 0 and 1. w is calculated by the method described in [37].

${P_{H,i}}^{(g-1)}$ in the last generation (i.e., $g-1$) is determined by the following:

$${P_{H,i}}^{(g-1)} = \begin{cases} P_i^{(g-1)} & \text{for } \mathrm{MSE}(P_i^{(g-1)}) < \mathrm{MSE}({P_{H,i}}^{(g-2)}) \\ {P_{H,i}}^{(g-2)} & \text{for } \mathrm{MSE}(P_i^{(g-1)}) \geq \mathrm{MSE}({P_{H,i}}^{(g-2)}). \end{cases} \tag{14}$$

$P_G^{(g-1)}$ is determined by the following:

$${P_G}^{(g-1)} = \underset{{P_{H,i}}^{(g-1)}}{\arg\min}\, \mathrm{MSE}({P_{H,i}}^{(g-1)}), \text{for } i = 1,\ 2,\ 3, \ldots, n. \tag{15}$$

Each particle P_i is then updated by

$$P_i^{(g)} = P_i^{(g-1)} + v_i^{(g)}. \tag{16}$$

If the updated value falls outside the boundary of the corresponding parameter, the velocity of the corresponding particle will be reversed in order to make the parameter fall within the search range.

The parameter set is perturbed to avoid the solution trapping into local optima. This can provide an opportunity of generating other possible solutions. Another particle $\tilde{P}_B^{(g)}$ is formed by introducing a perturbation $\delta p^{(g)}$ into the globally best particle $P_G^{(g)}$ before P_i is updated with (16). The perturbation is randomly generated from normal distribution with each parameter according to its searching boundary X_m individually. Thus, $\tilde{P}_B^{(g)}$ is calculated by the following:

$$\tilde{P}_B^{(g)} = P_G^{(g)} + \delta p^{(g)}. \tag{17}$$

Perturbation of each parameter m in the parameter set can be further expressed as follows:

$$\delta p^{(g)}(m) = (X_m^{\mathrm{Max}} - X_m^{\mathrm{Min}}) * \mathrm{Normal}(0, 0.64). \tag{18}$$

The Normal (0,0.64) is a random number of a normal distribution with a zero mean and 0.64 variance. X_m^{Max} is the upper boundary of parameter m and X_m^{Min} is the lower boundary of parameter m. Thus, the perturbation of parameter m at the gth generation $\delta p^{(g)}(m)$ is generated within its boundary.

Equation (18) introduces a solution out of the globally best solution. Again, this can avoid the entire estimation trapping into local optima. Then, the MSEs of $\tilde{P}_B^{(g)}$ and $P_G^{(g)}$ are computed with (11) and are compared. If $\mathrm{MSE}(\tilde{P}_B^{(g)}) < \mathrm{MSE}({P_G}^{(g)})$, $\tilde{P}_B^{(g)}$ is better than $P_G^{(g)}$. $P_G^{(g)}$ will be replaced by the best one in the set $\{P_G^{(g)} + \delta p^{(g)},\ P_G^{(g)} + 2\delta p^{(g)},\ P_G^{(g)} + 4\delta p^{(g)},\ \ldots,\ P_G^{(g)} + 2^j \delta p^{(g)}\}$, where $P_G^{(g)} + 2^j \delta p^{(g)}$ is within the search boundaries and $P_G^{(g)} + 2^{j+1}\delta p^{(g)}$ is outside the boundaries.

TABLE I
SEARCHING BOUNDARIES OF EACH PARAMETER

Parameter	Value		Parameter	Value	
	Min.	Max.		Min.	Max.
SOC(0)	0 %	100 %	τ_1	0.1 ms	1 s
R_0	$0.5R_0^*$	$1.5R_0^*$	τ_2	1 s	10 s
R_1, R_2	0.1mΩ	1 Ω	$v_1(0), v_2(0)$	-1.5 V	1.5 V

Note: R_0^* is the value obtained by (2).

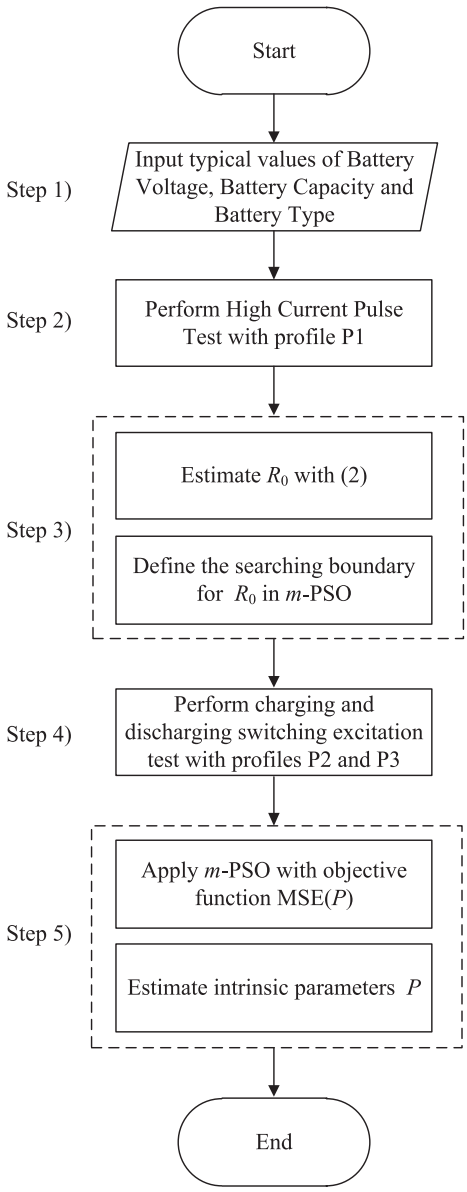

Fig. 5. Flowchart of the proposed system test.

That is

$$P_G^{(g)} = \arg\min_p \mathrm{MSE}(p), \text{subject to } :p = {P_G}^{(g)} + 2^r \delta p^{(g)} \tag{19}$$

where $r = 0, 1, 2, \ldots, j$.

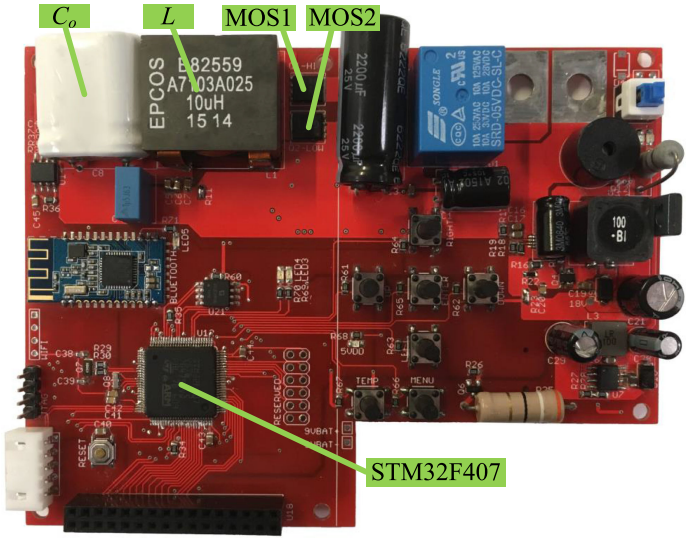

Fig. 6. Photo of the prototype.

TABLE II
VALUES OF MAJOR COMPONENTS

C_0 (F)	R_c (mΩ)	L (μH)	R_L (mΩ)	R_{sense} (mΩ)	P_{Rsense} (W)	R_{on} (mΩ)
2.5	56.8	10	2.4	0.25	4	2

Note: $P_{\mathrm{R\,sense}}$ is the power rating of the sensing resistor.

Apart from avoiding local optima, searching of the solution is accelerated with the local search in (19). The perturbation process simulates a self-generated new solution. The procedure of estimating the parameters is described as follows.

Step 1: All particles are randomly initialized with the parameters in each particle within their search boundaries determined by Table I. Thus, different from other methods, the initial guess in this m-PSO is randomly generated.

Step 2: The MSEs of all particles (candidates for P) are evaluated by (11).

Step 3: The new position and velocity of all particles are calculated by (16) and (13), respectively. A new particle $\tilde{P}_B^{(g)}$ is generated by introducing random perturbation in (17).

Step 4: The best particle in the swarm, $P_G^{(g)}$, will be replaced by the criterion in (19) if the condition of $\mathrm{MSE}(\tilde{P}_B^{(g)}) < \mathrm{MSE}({P_G}^{(g)})$ is met.

Step 5: The algorithm will go to Step 2) if the number of generation is less than σ.

V. TESTING PROCEDURE

With the help of Fig. 5, the intrinsic parameters of the battery under test are estimated by the following steps.

Step 1: Based on the battery information including battery voltage, capacity, and type, the v_{oc} - SOC characteristics are extracted with the method described in Section IV.

Step 2: The battery is subject to a high current discharging with the profile P1.

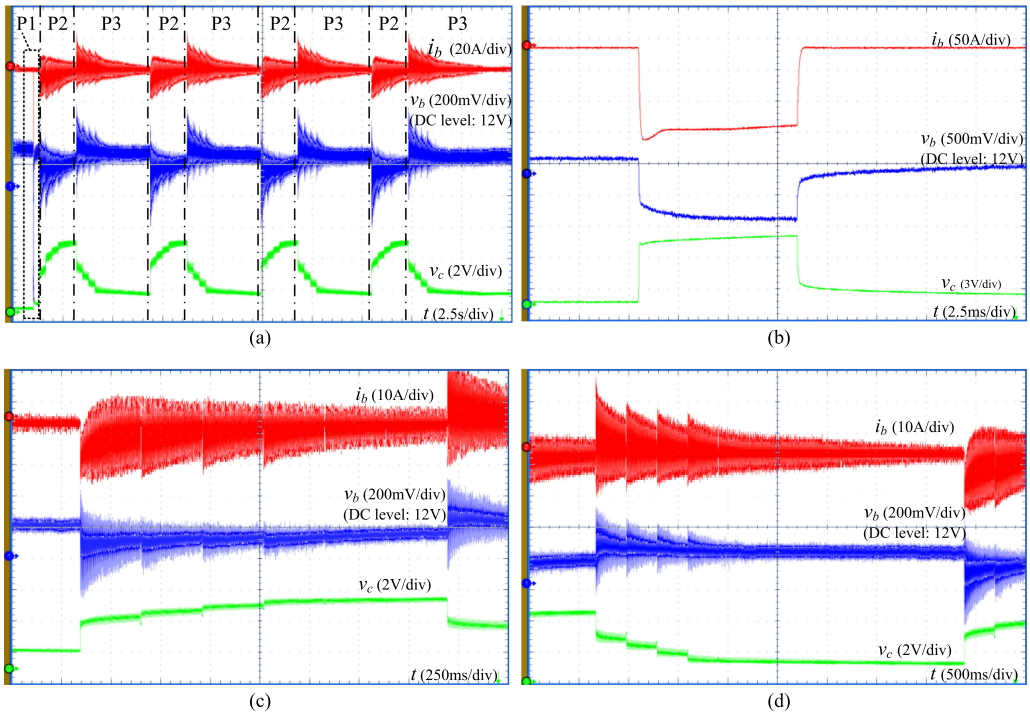

Fig. 7. Testing waveforms. (a) Overall waveforms. (b) Profile P1. (c) Profile P2. (d) Profile P3.

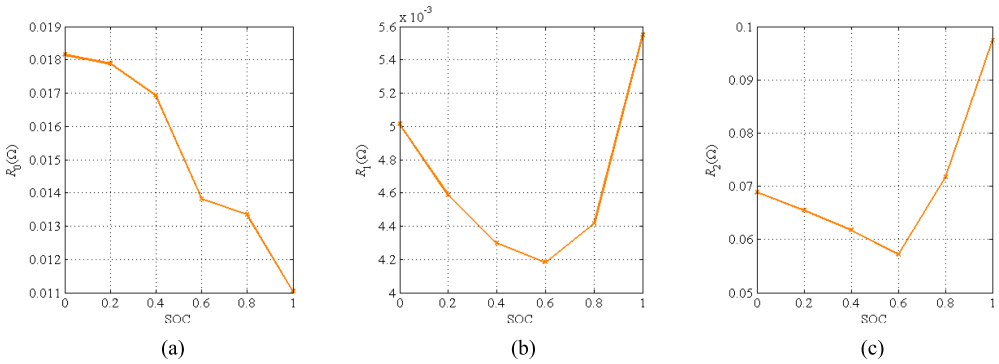

Fig. 8. Evolution of R_0, R_1, and R_2 against SOC.

Step 3: An approximated value of R_0 is calculated by (2) and the searching boundary of R_0 in m-PSO engine is also defined based on the approximated value.

Step 4: The battery is subject to discharging and charging tests with the profiles P2 and P3 alternately conducted for N times.

Step 5: The searching boundaries of other parameters, as given in Table I, and the voltage and current data sampled in conducting the profiles P2 and P3 are used to estimate the intrinsic parameters P with the BVE and m-PSO engine.

VI. Experimental Verification

A prototype that can test eight different types of batteries, as listed in Section IV, is shown in Fig. 6. The values of the major components are given in Table II. The controller is STMicroelectronics STM32F407. Fig. 7 shows the voltage and current waveforms in testing a 12 V, 60 Ah EFB - Varta D53. The duration of conducting profile P1 is 6 ms and the maximum testing current is 128 A. Profiles P2 and P3 are repeatedly conducted for four times, i.e., $N = 4$. The prototype takes 2 min to complete the estimation of the parameters listed in (6). Fig. 8 shows the evolution of the values of R_0, R_1, and R_2 against SOC. Results show that R_0 increases as the SOC decreases. R_1 and R_2 are higher, when SOC $= 1$ and SOC $= 0$.

The fitness of the estimated intrinsic parameters in the battery electrical model are verified by applying the current profile, as shown in Fig. 9(a), to the battery and comparing the predicted battery voltage waveform with the actual one. Fig. 9(b) shows the predicted and estimated voltage waveforms and their errors. Results show that the error is less than 0.4%. The round-trip efficiency of the prototype, which is defined as the energy delivered from the battery and the energy transferred back to the battery, is found to be 50%. In other words, about 50% of energy is recycled throughout the test. Thus, the mechanism allows to test the battery for a long period of time. The major losses of the

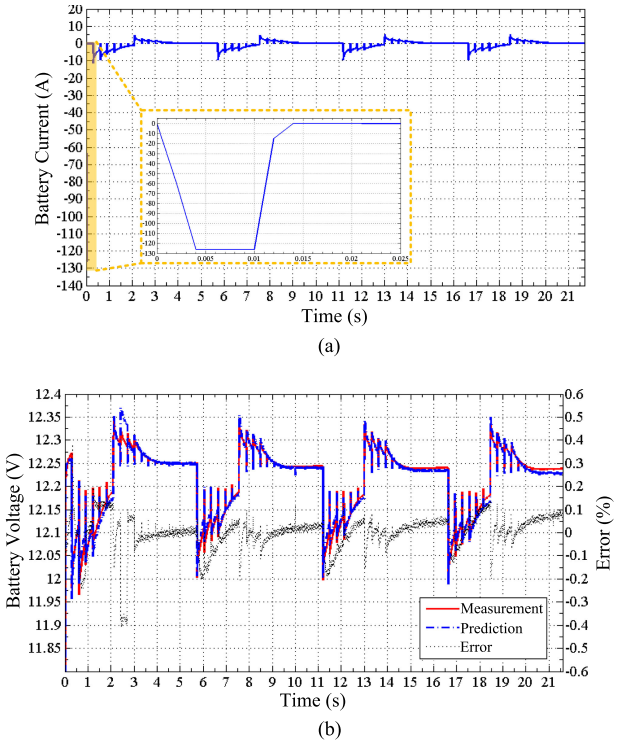

Fig. 9. Current profile, predicted and actual voltage waveforms, and errors. (a) Current profile. (b) Predicted and actual voltage waveforms, and errors.

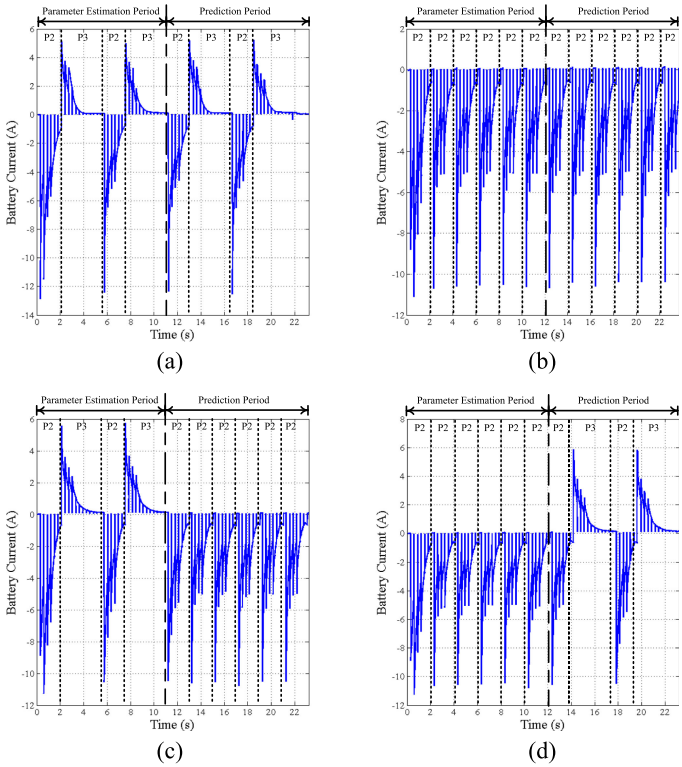

Fig. 10. Four different test cases. (a) TC1. (b) TC2. (c) TC3. (d) TC4.

prototype are due to the loss in the equivalent series resistance of the supercapacitor, charge and discharge efficiency of the supercapacitor. The power conversion efficiency of the bidirectional converter in conducting P2 is about 95% and that in conducting P3 is about 83%. The charge and discharge efficiency, i.e., round-trip efficiency, of the supercapacitor is found to be 64%.

The importance of extracting intrinsic parameters with both charging and discharging characteristics to predict battery charging and discharging characteristics is studied. Fig. 10 shows four different test cases, TC1–TC4. In TC1, the battery is first subject to profiled charging and discharging processes in estimating the intrinsic parameters. Then, the charging and discharging behaviors of the battery are predicted. In TC2, the battery is first subject to a profiled discharging process only in estimating the intrinsic parameters. Then, the discharging behavior of the battery is predicted. In TC3, the battery is first subject to profiled charging and discharging processes in estimating the intrinsic parameters. Then, the discharging behavior of the battery is predicted. Finally, in TC4, the battery is first subject to a profiled discharging process in estimating the intrinsic parameters. Then, the charging and discharging behaviors of the battery are predicted. The prediction results and errors in the four test cases are shown in Fig. 11. It can be concluded that the parameters estimated with both charging and discharging processes can give a higher accuracy in predicting in both charging and discharging behaviors. If the parameters is only estimated with the discharging process (TC2 and TC4), only the discharging behavior can be predicted accurately. For example, the prediction error in TC4 is higher than that in TC1.

Table III shows the estimated parameters in the four test cases. The estimated SOC(0) in TC1 and TC3 are 0.6558 and 0.6481, which are close to the theoretical value of 0.65, with errors of 0.89% and –0.29%, respectively. Conversely, the estimated values in TC2 and TC4 are 0.6722 and 0.6728, respectively, with higher errors of 3.42% and 3.5%, respectively. The errors are due to inaccurate estimations of the parameters of the *RC* networks with the discharging profiles only. For example, the estimated R_1 in TC2 and TC4 are 0.1 mΩ that reaches the minimum search boundary. The estimated R_1 in TC1 and TC3 are around 4.7 mΩ. The estimated value of R_0 in the four cases is compared with the reference value of 13.38 mΩ obtained by the method described in IEC 60896 [24]. The errors in TC1, TC2, TC3, and TC4 are $+3.2\%$, 7.62%, 2.16%, and 4.93%, respectively. The errors with unidirectional excitation is higher than that with bidirectional excitation. Based on [44], different sets of intrinsic parameters for describing the charging and discharging processes should be adopted. The inaccuracy of unidirectional excitation may further be explained by the redistribution rate of ions [45] upon charging and discharging process.

The variation of the discharging profile on estimating the intrinsic parameters is further investigated. Based on the discharging profile in TC2, four more profiles are derived. They are TC2a, TC2b, TC2c, and TC2d, as shown in Fig. 12.

In TC2a, battery relaxation periods (BR) are inserted between each two discharging profiles P2. The battery is first subject to the profiled discharging with relaxation process in estimating the intrinsic parameters. Then, the discharging behavior of the battery is predicted. In TC2b, the high-frequency current

TABLE III
PARAMETERS ESTIMATED IN THE FOUR TEST CASES

Test case	SOC(0)	R_0 (mΩ)	R_1 (Ω)	R_2 (Ω)	τ_1 (s)	τ_2 (s)	$v_1(0)$ (V)	$v_2(0)$ (V)	MSE (%)
TC1	0.6558	13.81	0.0047	0.0576	0.268	10	-0.0234	0.0031	0.0716
TC2	0.6722	14.40	0.0001	0.1185	0.97	9.98	-0.0231	-0.0024	0.0842
TC3	0.6481	13.67	0.0049	0.0633	0.271	10	-0.0309	0.0056	0.0809
TC4	0.6728	14.04	0.0001	0.1215	0.886	9.98	0.0165	-0.0293	0.1889

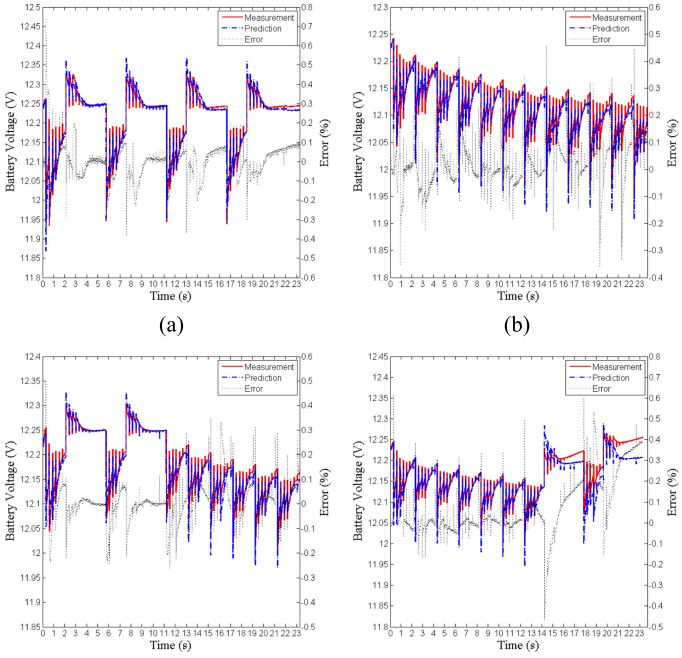

Fig. 11. Prediction results and errors in the four test cases. (a) TC1. (b) TC2. (c) TC3. (d) TC4.

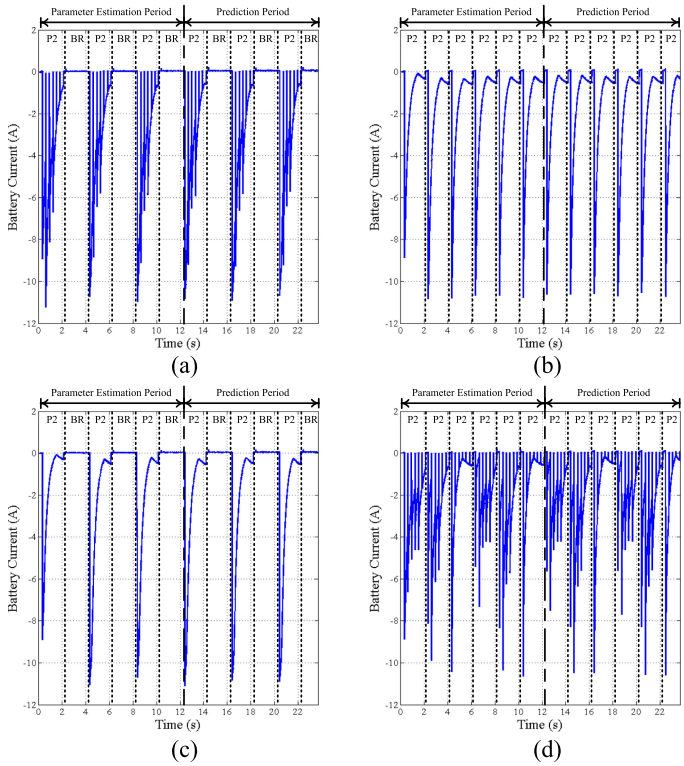

Fig. 12. Four different current profiles derived from TC2. (a) TC2a. (b) TC2b. (c) TC2c. (d) TC2d.

perturbations in the discharging profile P2 are removed such that the discharging profile consists of low-frequency components only. The battery is subject to the discharging process without high-frequency excitation in estimating the intrinsic parameters. Then, the discharging behavior of the battery is predicted. In TC2c, battery relaxation periods and low-frequency excitation have been both applied. The battery is first subject to the modified discharging process in estimating the intrinsic parameters. Then, the discharging behavior of the battery is predicted. Finally, in TC2d, three different amplitudes of profile P2 have been applied. The battery is subject to the combination of discharging pulses in estimating the intrinsic parameters. Then, the discharging behavior of the battery is predicted. The prediction results and errors of the battery voltage with the four discharging profiles are shown in Fig. 13. Results show that the parameters estimated with the four discharging profiles give a high accuracy in predicting the discharging behavior.

Table IV shows the estimated intrinsic parameters with the four current profiles. The RMS value of the MSE defined in (11) in all cases are less than 0.085%. The estimated SOC(0) with the profile TC2d is close to the theoretical value of 0.65 with an error of 1.17%. Conversely, the errors with profiles TC2a, TC2b, and TC2c are 6.03%, 8.14%, and 10.09%, respectively. The errors in estimating SOC(0) with TC2a and TC2c are higher than that with TC2 and TC2b. Thus, the duration of the BR is not a critical factor of improving the estimation accuracy.

High-frequency excitation in the profiles affects the accuracy in parameter extraction. For instance, the error in estimating SOC(0) with TC2b is higher than that with TC2. The current profile TC2d consists of both high- and low-frequency random pulses, providing rich information to extract the parameters. Thus, it gives accurate estimation of the value of SOC. Nevertheless, as shown in Fig. 14, the charging characteristics cannot be well predicted with the extracted parameters, confirming again the importance of estimating the parameters with both charging and discharging characteristics.

The value of R_0 obtained by the prototype is verified by comparing the measurement results with the high current pulse test described in [5] and the method described in IEC 60896

TABLE IV
ESTIMATED INTRINSIC PARAMETERS WITH DIFFERENT CURRENT PROFILES, TC2a–TC2d

Test case	SOC(0)	R_0 (mΩ)	R_1 (Ω)	R_2 (Ω)	τ_1 (s)	τ_2 (s)	$v_1(0)$ (V)	$v_2(0)$ (V)	MSE (%)
TC2a	0.6892	14.09	0.0016	0.0838	0.094	10	-0.0336	-0.0464	0.0812
TC2b	0.7029	14.55	0.0001	0.1387	0.106	9.99	-0.0168	-0.1354	0.0762
TC2c	0.7156	13.40	0.0063	0.0762	0.999	10	-0.0198	-0.074	0.0858
TC2d	0.6576	13.62	0.0048	0.0673	0.097	10	-0.0199	-0.0084	0.0817

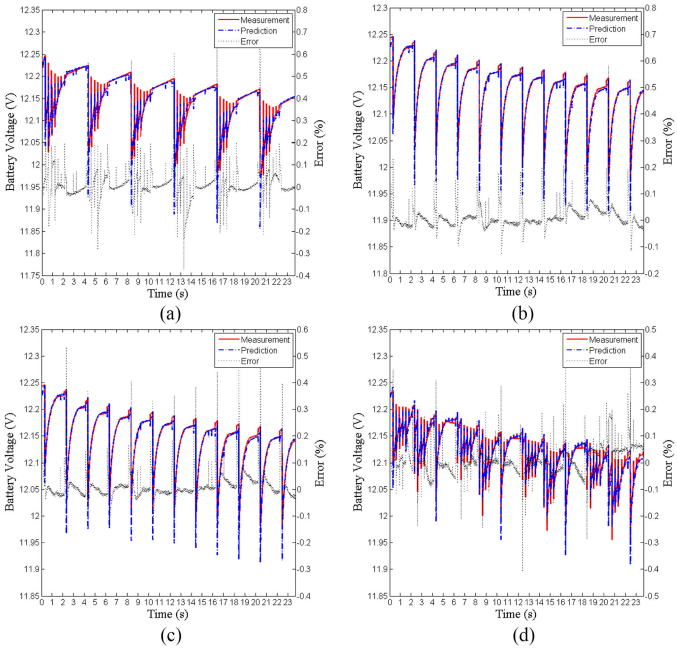

Fig. 13. Prediction results and errors in the four test cases derived from TC2. (a) TC2a. (b) TC2b. (c) TC2c. (d) TC2d.

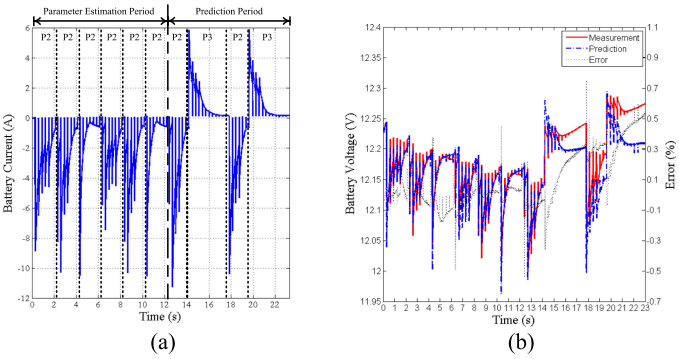

Fig. 14. Prediction results and errors with various discharging pulses current profile. (a) Current profile. (b) Predicted result and error.

standard [24] conducted on the battery test system NH Research 9210. The results are shown in Table V and are close to the value obtained by the IEC 60896 standard.

In order to compare the robustness and accuracy of m-PSO, the EKF has been implemented. The results obtained by the two methods are compared and shown in Fig. 15. The estimated SOC(0) with the two methods are compared with the theoretical

TABLE V
ESTIMATION RESULTS OF R_0 WITH DIFFERENT METHODS

Testing Method	Estimated / Measured R_0 (mΩ)	Error (%)
IEC 60896 standard [24]	13.38	0
130A current pulse test [5]	14.45	+8.0%
Prototype	13.81	+3.2%

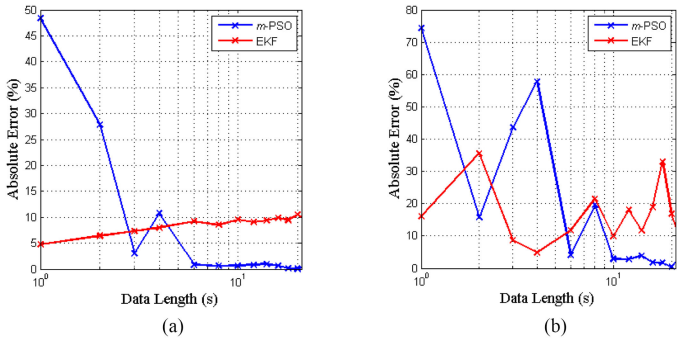

Fig. 15. Error of parameters with different estimation algorithms. (a) Error of SOC(0). (b) Error of R_0.

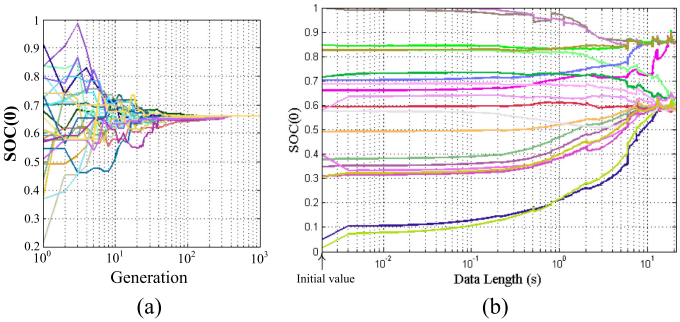

Fig. 16. Estimated SOC(0) versus generation and data length with m-PSO and EKF. (a) m-PSO. (b) EKF.

value of 0.65. The minimum error of SOC(0) obtained by the EKF and m-PSO are 4.7% and 0.35%, respectively. The estimated value of R_0 with the two methods is compared with the value of 13.38 mΩ, obtained by the method described in IEC 60896. The minimum errors obtained by the EKF and m-PSO are 4.89% and 0.52%, respectively. Thus, the accuracy of the m-PSO is higher than that of the EKF. Moreover, the EKF is highly dependent on the initial guess. Figs. 16 and 17 show the

TABLE VI
PARAMETERS ESTIMATED IN THE TWO TEST CASES

Test case	SOC(0)	R_0 (mΩ)	R_1 (Ω)	R_2 (Ω)	τ_1 (s)	τ_2 (s)	$v_1(0)$ (V)	$v_2(0)$ (V)	MSE (%)
DC	0.7820	8.08	0.0322	0.0135	0.0054	9.588	-0.0049	0.0818	0.0169
Arbitrary	0.5670	13.67	0.0204	0.0439	0.0008	10	0.0054	0.0527	0.3993

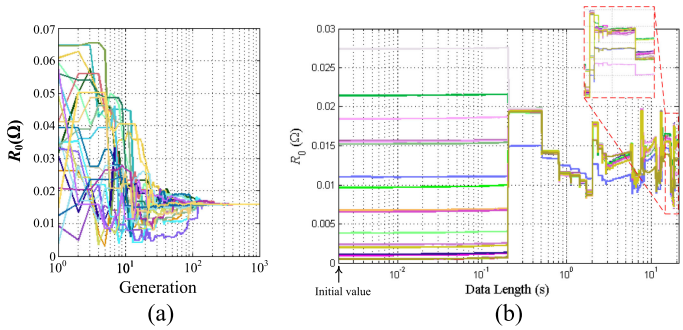

Fig. 17. Estimated R_0 versus generation and data length with m-PSO and EKF (a) m-PSO. (b) EKF.

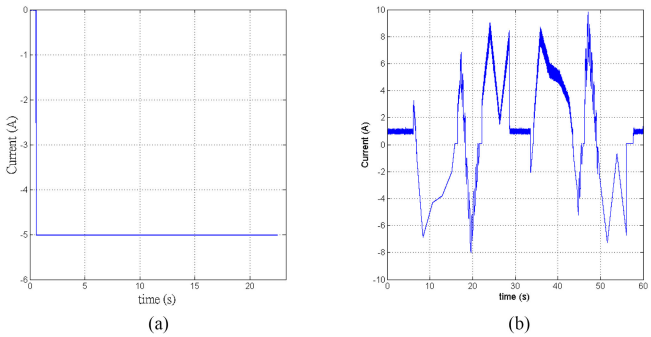

Fig. 18. Two different current profiles. (a) DC current. (b) Arbitrary current.

estimated parameters SOC(0) and R_0 versus generation and data length with two methods. The EKF can converge to different results if the initial values are different. While m-PSO does not have such issue, as it is a stochastic search algorithm.

VII. DISCUSSIONS

The effect of the battery current profile and the variation of the value of supercapacitor on the estimation accuracy, and indication of battery aging are discussed.

A. *Effect of the Battery Current Profile*

The proposed method does not limit to specific battery current waveform. After the time series of the actual battery voltage and current are recorded, a time series of the battery voltage will be estimated with the actual battery current, circuit model, and estimated values of the intrinsic parameters. Then, the estimated battery voltage will be compared with the actual battery voltage and their difference gives the m-PSO algorithm to generate new sets of parameters through several operators. Fig. 18 shows

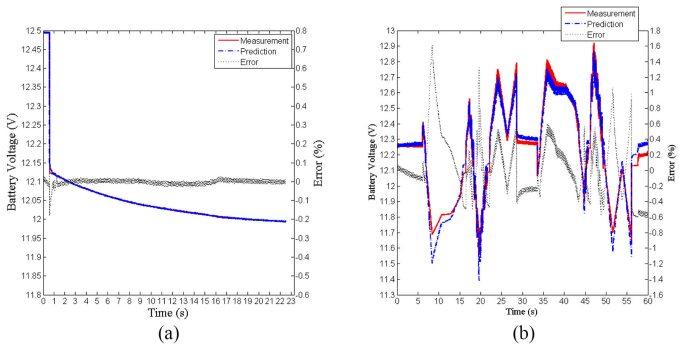

Fig. 19. Prediction results and errors in the two test cases. (a) DC. (b) Arbitrary.

TABLE VII
ESTIMATION RESULTS OF SOC(0) IN THE TWO TEST CASES

Test case	Reference value	Estimated / Measured SOC(0)	Error (%)
DC	0.8	0.7820	-2.25
Arbitrary	0.6	0.5670	+5.50

another two current profiles. They are 1) dc discharging current and 2) arbitrary current profile consisting of high- and low-frequency components. Fig. 19 shows the prediction results and errors. Results show that the estimated voltage response is close to the actual voltage in both cases. The maximum errors of the two cases are 1.08% and 1.62%, respectively. The estimated parameters under the two current profiles are shown in Table VI. The errors of SOC(0) estimated with the m-PSO are shown in Table VII.

B. *Effect of the Variation of the Value of the Supercapacitor*

As shown in Section III, the capacitance of supercapacitor C_0 only affects the maximum current pulse and the current amplitude during the discharging and charging processes. Fig. 20 shows the current profile when C_0 is 5 F, which is double the one used in prototype. The current amplitude is larger, but the value of C_0 does not affect the estimation of the values of the parameters as shown in Table VIII.

C. *Battery Aging*

Battery aging factors include corrosion in anode, irreversible sulfuration, acid stratification, and water loss [42], [46]. Among them, anodic corrosion is the major factor of reducing the conductivity of the electrode. Thus, the performance of a battery decreases, due to the increase in the internal resistance and the

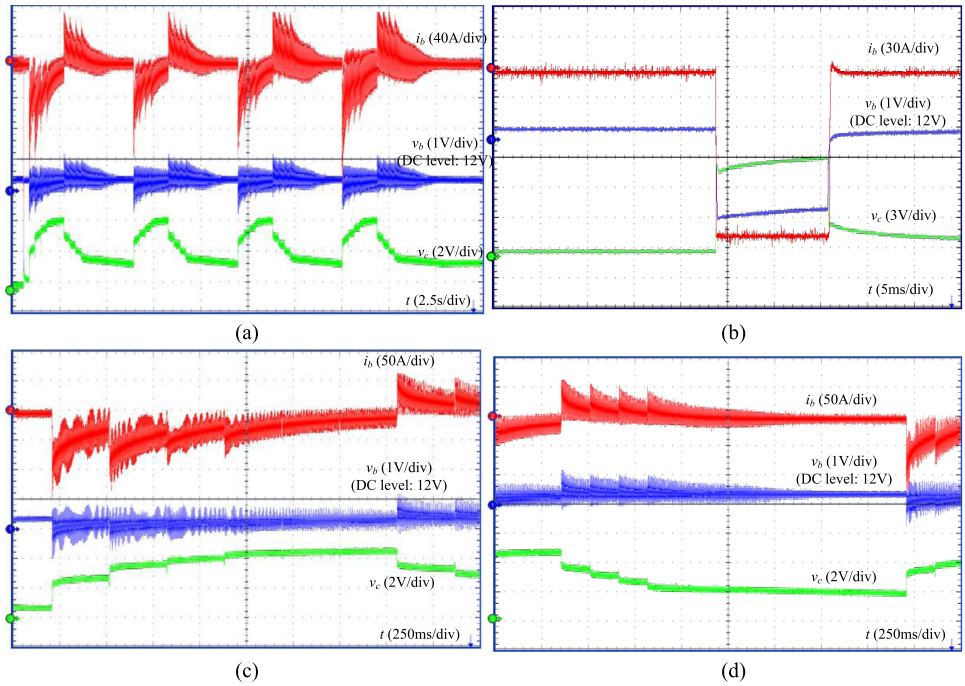

Fig. 20. Testing waveforms. (a) Overall waveforms. (b) Profile P1. (c) Profile P2. (d) Profile P3.

TABLE VIII
PARAMETERS ESTIMATED WITH TWO DIFFERENT VALUES OF C_0

C_0 (F)	SOC(0)	R_0 (mΩ)	R_1 (Ω)	R_2 (Ω)	τ_1 (s)	τ_2 (s)	$v_1(0)$ (V)	$v_2(0)$ (V)
2.5	0.67	12.73	0.0044	0.0080	0.0087	8.01	0.020	-0.03
1.25	0.67	12.72	0.0049	0.0069	0.0099	6.42	0.002	-0.04

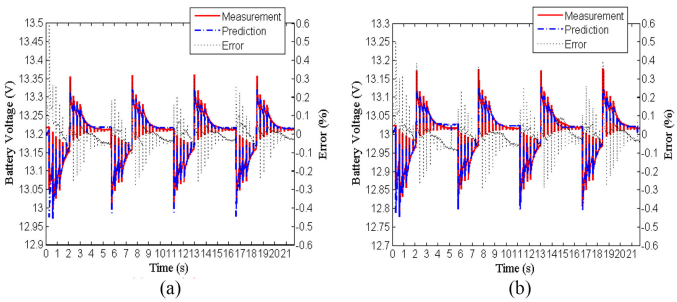

Fig. 21. Estimated results and errors. (a) Fresh battery. (b) Aged battery.

capacity loss. As the aging factor of batteries is reflected directly from the intrinsic parameters, the proposed method can be used to study aging. According to the battery aging studies in [30]–[32], the ohmic resistance will increase with the service time. The proposed method is able to estimate accurately the ohmic resistance R_0, implying that the battery aging can be identified. Fig. 21 shows two estimated results and errors of a fresh battery and aged battery. Table IX shows the values of R_0 obtained by the m-PSO and the method given in IEC 60896, respectively. It can be concluded that the proposed method can give indication on the battery life with the estimated intrinsic parameters.

TABLE IX
ESTIMATION RESULTS OF R_0 WITH FRESH AND AGED BATTERY

Testing Method	Battery	Estimated / Measured R_0 (mΩ)	Error (%)
IEC 60896 standard [24]	Aged	13.41	0
	Fresh	12.26	0
Prototype with m-PSO	Aged	13.55	+1.04
	Fresh	11.92	-2.77

The present design is more suitable for offline measurement, but it can be modified to conduct online measurement. Instead of measuring the current drawn by the proposed system with the sensing resistor R_{sense} in Fig. 1, the actual battery current is sensed with a current sensor. Thus, the time series of the actual battery current and actual battery voltage can be used to conduct the online estimation of the intrinsic parameters with the m-PSO.

VIII. CONCLUSION

An energy recycling technique for extracting the intrinsic parameters of lead–acid batteries has been presented. The charging and discharging processes are carried out by controlling the energy flow between the battery under test and a supercapacitor. By sampling the battery voltage and current during the processes, the intrinsic parameters are estimated. The estimation algorithm is based on an m-PSO algorithm that reduces the convergence time and the required data length with an internal resistance approximation method. Detailed implementations and performance have been given. A prototype that can estimate intrinsic parameters of eight different types of batteries have been built and evaluated. The testing results on a 12 V, 60 Ah EFB

have been given. The experimental results reveal that the proposed technique can effectively reduce energy consumption and provide accurate, and detailed information about the battery. In order to investigate the importance of using charging and discharging characteristics to estimate the intrinsic parameters, different testing profiles have been applied. Results show that the prediction results will be more accurate with both charging and discharging characteristics taken into the estimation. The estimated result with the prototype is favorably with the values obtained by other standard methods. Moreover, the proposed method m-PSO is compared with the EKF and the result shows m-PSO has better robustness and higher accuracy. As described in the cell capacity study in [30], the condition of battery can be analyzed by observing the change of R_0 with the proposed technique.

REFERENCES

[1] F. Ongaro, S. Saggini, and P. Mattavelli, "Li-ion battery-supercapacitor hybrid storage system for a long lifetime, photovoltaic-based wireless sensor network," *IEEE Trans. Power Electron.*, vol. 27, no. 9, pp. 3944–3952, Sep. 2012.

[2] A. Kuperman, I. Aharon, S. Malki, and A. Kara, "Design of a semi-active battery-ultracapacitor hybrid energy source," *IEEE Trans. Power Electron.*, vol. 28, no. 2, pp. 806–815, Feb. 2013.

[3] K. Ng, C. Mo, Y. Chen, and Y. Hsieh, "State-of-charge estimation for lead-acid batteries based on dynamic open-circuit voltage," in *Proc. IEEE 2nd Int. Power Energy Conf.*, 2008, pp. 972–976.

[4] M. Coleman, C. K. Lee, C. Zhu, and W. G. Hurley, "State-of-charge determination from EMF voltage estimation: Using impedance, terminal voltage, and current for lead-acid and lithium-ion batteries," *IEEE Trans. Ind. Electron.*, vol. 54, no. 5, pp. 2550–2557, Oct. 2007.

[5] M. Coleman, C. Lee, and W. Hurley, "State of health determination: two pulse load test for a VRLA battery," in *Proc. 37th IEEE Power Electron. Spec. Conf.*, 2006, pp. 1–6.

[6] A. Mejdoubi, A. Oukaour, H. Chaoui, H. Gualous, J. Sabor, and Y. Slamani, "State-of-charge and state-of-health lithium-ion batteries' diagnosis according to surface temperature variation," *IEEE Trans. Ind. Electron.*, vol. 63, no. 4, pp. 2391–2402, Apr. 2016.

[7] W. Huang and J. Qahouq, "An online battery impedance measurement method using DC–DC power converter control," *IEEE Trans. Ind. Electron.*, vol. 61, no. 11, pp. 5987–5995, Nov. 2014.

[8] J. D. Kozlowski, "A novel online measurement technique for AC impedance of batteries and other electrochemical systems," in *Proc. 16th Annu. Battery Conf. Appl. Adv.*, 2001, pp. 257–262.

[9] R. S. Robinson, "System noise as a signal source for impedance measurements on battery connected to operating equipment," *J. Power Sources*, vol. 42, no. 3, pp. 381–388, Feb. 1993.

[10] J. P. Christophersen, C. H. Motloch, J. Morrison, I. Donnellan, and W. Morrison, "Impedance noise identification for state-of-health prognostics," in *Proc. 43rd Power Sources Conf.*, Jul. 2008.

[11] F. Huet, "A review of impedance measurements for determination of the state-of-charge or state-of-health of secondary batteries," *J. Power Sources*, vol. 70, no. 1, pp. 59–69, 1998.

[12] P. Wu, W. Hsu, and J. Chen, "Detection on SOC of VRLA battery with EIS," in *Proc. 1st Int. Future Energy Electron. Conf.*, 2013, pp. 897–902.

[13] C. Gabrielli, "Identification of electrochemical processes by frequency response analysis," Solartron Anal. Group, Hampshire, U.K., Tech. Rep. 004/83, Mar. 1998.

[14] A. Blidberg, "Correlation between different impedance measurement methods for battery cells," KTH Chem. Sci. Eng. Degree Project, Stockholm, Sweden, 2012.

[15] H. Blanke *et al.*, "Impedance measurements on lead-acid batteries for state-of-charge, state-of-health and cranking capability prognosis in electric and hybrid electric vehicle," *J. Power Sources*, vol. 144, no. 2, pp. 418–425, Jun. 2005.

[16] M. Greenleaf, H. Li, and J. Zheng, "A temperature-dependent study of sealed lead-acid batteries using physical equivalent circuit modeling with impedance spectra derived high current/power correction," *IEEE Trans. Sustain. Energy*, vol. 6, no. 2, pp. 380–387, Jan. 2015.

[17] J. Morrison and W. Morrison, "Method of delecting system function by measuring frequency response," U.S. Patent 7,395,163 B1, Jul. 2008.

[18] C. Yoon, Y. Barsukov, and J. Kim, "Method of and Apparatus for measuring battery capacity by impedance spectrum analysis," U.S. Patent 6,208,147 B1, Mar. 2008.

[19] J. P. Christophersen, J. Morrison, W. Morrison, and C. Motloch, "Rapid impedance spectrum measurements for state-of-health assessment of energy storage devices," *SAE Int. J. Passenger. Cars, Electron. Electr. Sys.*, vol. 5, no. 1, pp. 246–256, May 2012.

[20] A. Waligo and P. Barendse, "A comparison of the different broadband impedance measurement techniques for lithium-ion batteries," in *Proc. IEEE Energy Convers. Congr. Expo.*, 2016, pp. 1–7.

[21] C. Beer, P. Barendse, and P. Pillay, "Fuel cell condition monitoring using optimized broadband impedance spectroscopy," *IEEE Trans. Ind. Electron.*, vol. 62, no. 8, pp. 5306–5316, Apr. 2015.

[22] J. Shim and K. A. Striebel, "Characterization of high-power lithium-ion cells during constant current cycling part I. Cycle performance and electrochemical diagnostics," *J. Power Sources*, vol. 122, no. 2, pp. 188–194, 2003.

[23] PNGV Battery Test Manual, INEEL, Cuernavaca, Mexico, DOE/ID-10597, Rev. 3, Feb. 2001.

[24] *Stationary Lead-Acid Batteries – Part 21: Valve Regulated Types – Methods of Test*, IEC 60896-21, 2004.

[25] *Electrically Propelled Road Vehicles – Test Specification for Lithium-Ion Traction Battery Packs and Systems*, ISO 12405-1, 2011.

[26] R. Li, J. Yu, J. Li, and F. Chen, "Equivalent model and parameter identification of lithium-ion battery," in *Proc. Chin. Intell. Automat. Conf.*, 2015, pp. 29–39.

[27] D. Stroe, M. Swierczynski, S. Kaer, and R. Teodorescu, "A comphrehensive study on the degradation of lithium-ion batteries during calendar ageing: the internal resistance increase," in *Proc. Energy Convers. Congr. Expo.*, 2016, pp. 1–7.

[28] J. Christophersen, "Battery state-of-health assesment using a near real-time impedance measurement technique under no-load and load conditions," thesis, , Montana State Univ., Bozeman, MT, USA, 2011.

[29] V. Pop, J. Bergveld, D. Danilov, P. P. L. Regtien, and P. H. L. Notten, *Battery Management System: Accurate State-of-Charge Indication for Battery-Powered Applications*. New York, NY, USA: Springer, 2008.

[30] E. Davis, D. Funk, and W. Johnson, "Stationary battery monitoring by internal ohmic measurements," Elect. Power Res. Inst., Palo Alto, CA, USA, Tech. Rep. 1002925, Dec. 2002.

[31] J. M. Hawkins and R. G. Hand, "AC impedance spectra of field-aged VRLA batteries," in *Proc. 18th Int. Telecommun. Energy Conf.*, 1996, pp. 640–645.

[32] E. Martinez-Laserna *et al.*, "Evaluation of lithium-ion battery second life performance and degradation," in *Proc. IEEE Energy Convers. Congr. Expo.*, 2016, pp. 1–7.

[33] M. A. Badamchizadeh, N. Nikdel, and M. Kouzehgar, "Optimization of data fusion method based on kalman filter using genetic algorithm and particle swarm optimization," in *Proc. 2nd Int. Conf. Comput. Automat. Eng.*, 2010, pp. 359–363.

[34] A. Klintberg, T. Wik, and B. Fridholm, "Theoretical bounds on the accuracy of state and parameter estimation for batteries," in *Proc. Amer. Control Conf.*, 2017, pp. 4035–4041.

[35] F. Kocadag, R. F. Cinar, and A. Demirkol, "Kalman filter and particle swarm optimization on real time satellite tracking," in *Proc. CIE Int. Conf. Radar*, 2016, pp. 1–5.

[36] R. Janapati, Ch. Balaswamy, and K. Soundararajan, "Enhanced mechanism for localization in wireless sensor networks using PSO assisted extended kalman filter algorithm (PSO-EKF)," in *Proc. Intern. Conf. Commun. Inf. Comput. Technol.*, 2015, pp. 1–6.

[37] W. Wang, H. Chung, and J. Zhang, "Near-real-time parameter estimation of an electrical battery model with multiple time constants and SOC-dependent capacitance," *IEEE Trans. Power Electron.*, vol. 29, no. 11, pp. 5905–5920, Nov. 2014.

[38] H. H. Afshari, M. Attari, R. Ahmed, M. Farag, and S. Habibi, "Modeling, parameterization, and state of charge estimation of li-ion cells using a circuit model," in *Proc. IEEE Transp. Electrific. Conf. Expo*, 2016, pp. 1–6.

[39] L. Juang, P. Kollmeyer, R. Zhao, T. Jahns, and R. Lorenz, "The impact of DC bias current on the modeling of lithium iron phosphate and lead-acid batteries observed using electrochemical impedance spectroscopy," in *Proc. IEEE Energy Convers. Congr. Expo.*, 2014, pp. 2575–2581.

[40] Z. He, G. Yang, H. Geng, N. Shen, and Z. Wang, "A battery modeling method and its verification in discharge curves of lead-acid batteries," in *Proc. IEEE Veh. Power Propulsion Conf.*, 2013, pp. 1–5.

[41] T. Sritharan, D. Yan, F. Dawson, and K. Lian, "Characterizing battery behavior for time-dependent currents," *IEEE Trans. Ind. Appl.*, vol. 50, no. 6, pp. 4090–4097, Mar. 2014.
[42] E. Ebner, M. Gelbke, E. Zena, M. Wieger, and A. Borger, "Temperature-dependent formation of vertical concentration gradients in lead-acid-batteries under pSOC operation – Part 2: sulfate analysis," *Electrochim. Acta*, vol. 262, pp. 144–152, Feb. 2018.
[43] N. Mohan, T. Undeland, and W. Robbins, *Power Electronics: Converters, Applications, and Design*, 3rd ed. Hoboken, NJ, USA: Wiley, 2003.
[44] A. Borger *et al.*, "Impedance spectra of enhanced flooded batteries for micro-hybrid applications," *J. Energy Storage*, vol. 13, pp. 457–462, Oct. 2017.
[45] H. Arora, R. S. Sherratt, B. Janko, and W. Harwin, "Experimental validation of the recovery effect in batteries for wearable sensors and healthcare devices discovering the existence of hidden time constants," *J. Eng.*, vol. 2017, no. 10, pp. 548–556, Oct. 2017.
[46] Ruetschi. "Aging mechanisms and service life of lead–acid batteries," *J. Power Sources*, vol. 127, nos. 1/2, pp. 33–44, Mar. 2004.

Chun-Sing Cheng (S'16) received the B.Eng. degree in computer engineering (business intelligence minor), in 2013, from the City University of Hong Kong, Kowloon, Hong Kong, where he is currently working toward the M.Phil. degree in electronic engineering.

His current research interests include battery modeling and battery diagnosis.

Ricky Wing-Hong Lau (M'88–SM'06) received the B.Sc. and Ph.D. degrees in electrical and electronic engineering from the University of Portsmouth, Portsmouth, U.K., in 1985 and 1989, respectively.

In 1990, he joined the Department of Electronic Engineering, City University of Hong Kong, Hong Kong, where he is currently an Associate Professor. His current research interests include digital signal processing, digital audio engineering, pulsewidth modulation spectrum analysis, embedded system design, and smart-grid development.

Dr. Lau was the recipient of the IEEE Third Millennium Medal. He was the Chairman of the IEEE Hong Kong Section in 2005.

Nand Kishor Rathi received B.E. degree in mechanical engineering from National Institute of Technology, Durgapur, India, in 1982, and PGDIT (Post Graduate Diploma in International Trade) degree from the Indian Institute of Foreign Trade, New Delhi, India, in 1985.

After briefly working in the field of Steel industry, he was engaged in international trading since 1985. Since 2006, he has been engaged in research and developments of battery management solutions. His current research focuses on battery diagnosis. He holds several patents in the field of efficient battery charging products. He has successfully launched several ac/dc and dc/dc chargers for automotive industry in international markets.

Henry Shu-Hung Chung (M'95–SM'03–F'16) received the B.Eng. and Ph.D. degrees in electrical engineering from the Hong Kong Polytechnic University, Hong Kong, in 1991 and 1994, respectively.

Since 1995, he has been with the City University of Hong Kong, where he is currently a Professor with the Department of Electronic Engineering and the Director of the Center for Smart Energy Conversion and Utilization Research. His current research interests include renewable energy conversion technologies, lighting technologies, smart grid technologies, and computational intelligence for power electronic systems. He has edited one book, authored eight research book chapters, and more than 400 technical papers including 180 refereed journal papers in his research areas, and holds 50 patents.

Dr. Chung was the Chair of the Technical Committee of the High-Performance and Emerging Technologies, IEEE Power Electronics Society in 2010–2014. He is currently the Editor-in-Chief of the IEEE POWER ELECTRONICS LETTERS and the Associate Editor of the IEEE TRANSACTIONS ON POWER ELECTRONICS and the IEEE JOURNAL OF EMERGING AND SELECTED TOPICS IN POWER ELECTRONICS. He was the recipient of numerous industrial awards for his invented energy saving technologies.